Solar Energy 206 (2020) 68–83

Contents lists available at ScienceDirect

Solar Energy

journal homepage: www.elsevier.com/locate/solener

A novel solar integrated distillation and cooling system – Design and analysis

Ahmad K. Sleiti*, Wahib A. Al-Ammari, Mohammed Al-Khawaja

Department of Mechanical & Industrial Engineering, College of Engineering, Qatar University, Qatar

ARTICLE INFO

Keywords:
Solar cooling
Solar distillation
Ejector
Refrigerants
Still productivity

ABSTRACT

To meet the high cooling and fresh water demands in hot and arid regions, a novel integrated solar cooling and solar distillation system is introduced. The system consists of a solar ejector cooling system integrated with single-slope solar still. The proposed novel system is the first study to integrate two solar systems for cooling and water production with outputs significantly higher than any existing system. A steady state thermodynamics model is developed based on the mass, momentum and energy conservations and the performance of the integrated system is investigated. Results showed that the productivity of the solar still is enhanced by increasing the evaporation rate (using heating coil) and by increasing the condensation rate (using cooling coil). Simultaneously, this improved the COP of the ejector system by enhancing its entrainment ratio with slight increase in the required solar collector area. The performance of the system is investigated further for four different scenarios of integration between the solar ejector cooling and solar distillation systems. Results showed that the productivity of the still is five times higher than that of the conventional solar still. The effects of the major operating parameters on the performance of the system with R134a as the working fluid are investigated and analyzed. At a solar radiation of 500 W/m^2, generator pressure of 3.3 MPa, generator temperature of 365 K, evaporator temperature of 283 K, a cooling capacity of 10.4 kW and distilled water of 8.10 kg/day are obtained. The annual produced water considering the hourly variation of the radiant flux was 5067 kg/year, which is 5.7 times more than the conventional systems. The estimated cost of one liter distilled water per 1 m^2 area of the present solar still is $0.04, which is only 18% of the water cost of other still technologies. Moreover, the performance of additional four working fluids is compared in terms of COP, cooling capacity, required solar collector area and still productivity, based on which, R134a working fluid was recommended for its overall performance.

1. Introduction

In hot climate regions, cooling demand has the largest share of the consumed energy and contributes the most to the peak load of the grid (Shublaq and Sleiti, 2020). At the same time, these regions usually suffer from shortage of sustainable potable water resources (Kumar and Martin, 2014). However, these regions receive relatively high intensity of solar radiation energy that could be harnessed to operate an integrated cooling and water production system with superior performance potential, which is the main goal of the present study. The integrated system may consist of an air conditioning system, using solar cooling technology, and a fresh water production system, using distillation technology (Abdel-Rehim and Lashine, 2012; Ghali et al., 2010). There are several solar cooling technologies that have been proposed in open literature including thermoelectric (Daghigh and Khaledian, 2018), photovoltaics (PV) modules (Opoku et al., 2018), absorption (Xu and Wang, 2018), adsorption (Pan et al., 2019), and ejector systems (Al-Nimr et al., 2020). Similarly, many solar distillation technologies have been studied with different designs and various enhancement techniques (Das et al., 2020).

The advantages of solar ejector cooling technology include its simplicity and its low cost compared to the other solar technologies (Zeyghami et al., 2015). This is particularly true in comparison, for instance to the cost of the thermoelectric cooling that is high relative to other technologies in addition to that fact that their cooling capacity is limited (Daghigh and Khaledian, 2018). The absorption refrigeration systems are suitable for large and commercial cooling systems, otherwise, the large size of their units, safety, and maintenance issues make them undesirable option (Alobaid et al., 2017). The PV technology could and is certainly being used to power conventional electrical

* Corresponding author.
E-mail address: asleiti@qu.edu.qa (A.K. Sleiti).

https://doi.org/10.1016/j.solener.2020.05.107
Received 15 April 2020; Received in revised form 28 May 2020; Accepted 31 May 2020
Available online 06 June 2020

Nomenclature

Symbols

A	area [m^2]
a	speed of the sound [m/s]
cp	specific heat [J/kg.K]
d	diameter [m]
G	solar radiation intensity [W/m^2]
Gr	Grashof number
h	specific enthalpy [J/kg.K]
h	the convective heat transfer coefficient [$W/m^2.K$]
k	thermal conductivity [W/m.K]
L	length [m]
M	Mach number
$\dot{m}$	mass flow rate [kg/s]
N	number of sun shining hours per day [h]
P	pressure [Pa]
Pr	Prandtl number
Q	heat transfer rate [W]
R	gas constant [J/kg.K]
T	temperature [K]
V	velocity [m/s]

Greek symbols

η	efficiency [%]
γ	specific heat ratio
φ	coefficient of frictional losses
ω	entrainment ratio
τ	transmittivity of the glass
α	absorptivity of saline water
ε	Emissivity

Subscripts

1, 2, t, m, c, g, p, e,…	states and positions presented in Fig. 1, Fig. 2, and Fig. 4
A	to ambient air
c,gl-a	of convection from the glass cover to the ambient air
co,ss	of cooling coil in the condenser chamber of the solar still
c,sw-gl	of convection from saline water to the glass cover
Ej	ejector system
ev, sw-gl	of evaporation from the saline water to the glass cover
Gl	of the glass cover
h,ss	of heating coil in the basin of the solar still
r,sw-gl	of radiation from saline water to the glass cover
r,gl-sky	of radiation from the glass cover to the sky
Sc	of the solar collector
Sky	of the sky
Sw	of the saline water

Abbreviations

COP	Coefficient of performance
CSS	Conventional Solar Still
GWP	Global warming potential
ODP	Ozone depletion potential
PBP	Payback period in years
S1	Scenario 1: ejector system isn't coupled with solar still system
S2	Scenario 2: ejector system is coupled with solar still system via heating coil
S3	Scenario 3: ejector system is coupled with solar still system via cooling coil
S4	Scenario 4: ejector system is coupled with solar still system via heating and cooling coils
SES	Solar ejector system
SSS	Solar still system

refrigeration and air conditioning systems, however, the high cost of their storage batteries forms a major barrier for their applications (Hasanuzzaman et al., 2016). Another attractive advantage of the ejector systems that makes them the preferable choice in the present study, is that they can be powered by ultra-low temperature heat source achievable by using solar evacuated tube collectors (Zhang et al., 2012) or using the available thermal energy from several waste heat resources (Petrenko et al., 2011).

On the negative side, the solar ejector cooling systems have relatively low Coefficient of Performance (COP); usually less than 1 and the operation of the ejector is not stable at off-design conditions. For these reasons, numerous studies have been conducted to improve the performance of the ejector as a component or as a cooling system (Tashtoush et al., 2019a). As a component, the performance of the ejector can be improved by optimizing its design parameters. It is found that the position of primary nozzle exit is the most important factor that affects the performance of the ejector (Yan et al., 2016; Pounds et al., 2013; Zhu et al., 2009). Other parameters including area ratio, length of mixing section, shape of the nozzle exit, angle of converging section, geometry of the mixing section, and diffuser size also have significant effects on the performance of the ejector (Yapici et al., 2008; Jia and Wenjian, 2012; Wu et al., 2014). Modifying the ejector geometry is another approach for its improvement as a component. For instance, dual-nozzle ejectors (Zhu et al., 2014; Zhou et al., 2013) and variable-geometry ejectors (Gutiérrez and León, 2014; Chen et al., 2017c) are example of this approach.

As a system, the design and ejector performance are inherently affected by the operating conditions, which are mainly the generator, evaporator, and condenser pressures and temperatures (Yan et al., 2017). An ejector can be designed to perform well at specified operating conditions (design conditions, but as these conditions change, its performance rapidly deteriorates. To address this, many researchers conducted theoretical and experimental studies to find out the relationships between the main operating conditions and the ejector design and performance. However, more advanced technologies that could achieve a performance improvement within the whole operation range are proposed. For instance, (Tang et al., 2017; Tang et al., 2018c) have proposed auxiliary entrainment and combined auxiliary entrainment technologies to suck more entrained steam. Also, they used pressure regulation technologies to optimize the entrainment passage of the blocked entrained flow, as well as the combined pressure regulation (Tang et al., 2018a, 2018b). Furthermore, Tang et al have presented visualization experimental study of the condensing flow regime in the transonic mixing process of desalination-oriented steam ejector (Tang et al., 2019). This study is important for reduction of internal irreversible losses and tailoring ejector design, as well as refining and evaluating physical and mathematical two-phase flow models of steam ejectors. Another key factor for enhancing the overall performance of the ejector cooling system, is the selection and the choice of the working fluid. Several studies have investigated the performance of several working fluids in ejector cooling system. Based on the range of the operating conditions, different working fluids have been

recommended (Chen et al., 2014; Chen et al., 2017b).

Regarding the solar distillation technologies, there are numerous studies that attempted to improve the performance of the domestic solar still units. These improvements can be briefly classified into four approaches: a) changing the operating mode of the still from passive to active operation (Manokar et al., 2018), b) changing the geometry of the still (such as double-slope, tubular, spherical, and pyramidic solar stills) (Kabeel et al., 2020), c) enhancing the evaporation rate by integrating with solar collector (Sathyamurthy et al., 2017), using phase change materials (Abu-Arabi et al., 2020; Al-harahsheh et al., 2018), and d) enhancing the condensation rate by cooling the glass cover, adding finned condensation chamber, using thermoelectric cooler modules, and by multi-effect condensation (Omara et al., 2017). However, most of these techniques, while only slightly improved the solar still productivity, they resulted in increasing the cost of distillation and adding more complexities compared to the conventional solar still.

The integration of the solar still with other heating, cooling, and power generation systems is another method to boost the overall efficiency of the solar system. Only few studies, found in open literature, investigated the enhancement of the still productivity by integration with air conditioning/cooling system. Ghali et al. (2010) theoretically studied the integration of a solar still with a conventional air condition system. They attempted to optimize the operation of the system for minimum energy consumption, while meeting the cooling and fresh water need of a residential space in the suburbs of Beirut. They reported that the cost of freshwater production of the combined system is 0.108 kWh/ liter for the month of August and 0.12 kWh/liter of fresh water in October. Another study of a combined solar still with a conventional air condition system is introduced by Abdel-Rehim et al (Abdel-Rehim and Lashine, 2012). They conducted an experimental study using a system composed of a 1 m^2 conventional solar still, 2.5 HP compressor with R22 as the working fluid, rectangular condenser with 54.5 × 61 cm^2 dimensions and evaporator cooling coil that is rectangular with 30.5 × 104 cm^2 dimensions. They reported a maximum freshwater productivity of only 29 Liters in daytime of June 5, 2009.

From the above discussion, it is clear that the available in open literature studies and technologies of integrated cooling and freshwater production systems are very limited and suffer from low COP and low water productivity. In the present study, however the performance of the solar still system is improved significantly by enhancing the evaporation and condensation rates via integration with solar ejector cooling system. The novelty of the present study is that (1) this integration of the ejector and still systems has not been introduced before in open literature; (2) in contrasts to studies in open literature, the two integrated systems are both solar and (3) the outputs (cooling effect and water productivity) of the proposed system are significantly higher than any existing system. The heat addition is enhanced by passing the hot working fluid of the ejector system through the solar still basin before entering the primary port of the ejector. While the heat removal is enhanced by passing the cold working fluid of the ejector through the condensing chamber of the still. This way, the performance of both systems is boosted with only slight increase in the required solar collector area and the condenser load compared to the unintegrated systems. The present study is organized in several sections; the system description and its operating mechanism is presented in Section 2. The thermodynamics model of the ejector and the solar still systems is developed based on the momentum, energy, and mass balance principles and is explained in Section 3. The effects of the major parameters including the generator pressure and temperature, evaporator temperature, solar radiation intensity and the used working fluids are discussed in detail in Section 4.

2. System description

Fig. 1 shows a schematic diagram of the proposed system. It consists of solar ejector system (SES) integrated with solar still system (SSS). The ejector system (right hand side of Fig. 1) is composed of cooling equipment including the condenser, expansion valve, evaporator and ejector device. The ejector works as a compressor to raise the pressure of the evaporator working fluid to the condenser pressure. The working fluid is condensed in the condenser (state 4) and then splits into primary (state 5) and secondary (state 7) flows. The secondary fluid flow is throttled in the expansion valve then evaporates in the evaporator by absorbing heat from the air of the air-conditioned space. The saturated temperature of the evaporator in the ejector cooling and air conditioning systems is usually designed within the range of 278–283 K (Saengmanee, 2017). The working fluid at this temperature range can be used for further cooling. So, it passes through the condensing

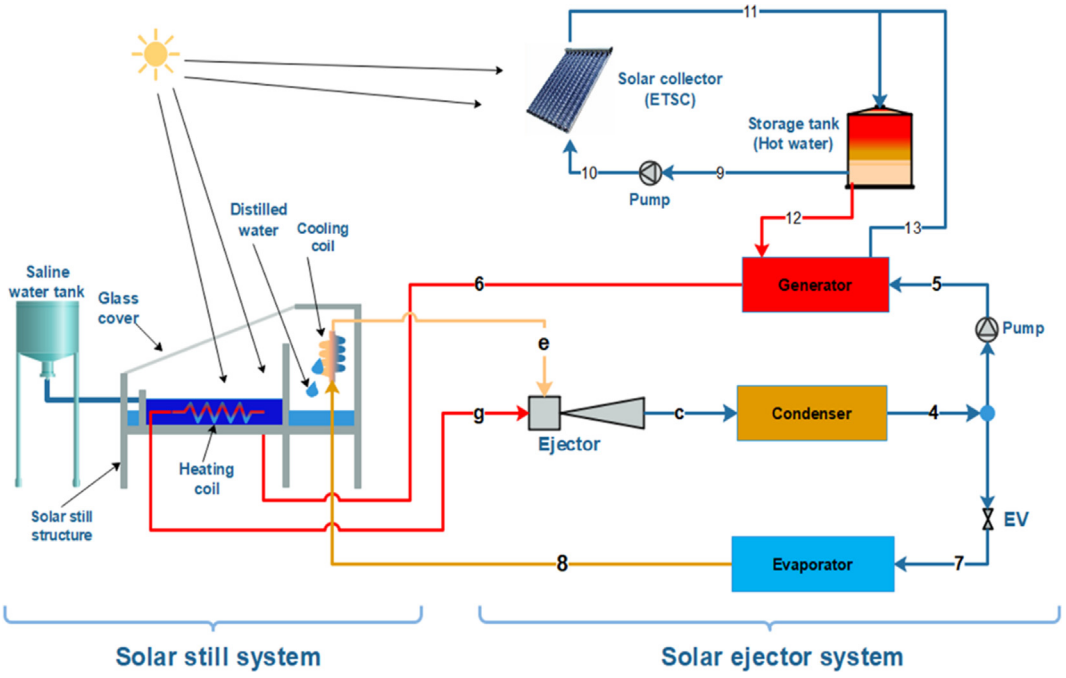

Fig. 1. Schematic diagram of the proposed system.

chamber of the solar still system to enhance the condensation of the freshwater vapor. Then the secondary working fluid is proceeded to the ejector (state e) to be compressed to the condenser pressure and then the process is repeated. The primary fluid flow (state 5) is pumped to high pressure by the pump and heated to supercritical conditions inside the generator. The high-pressure primary flow then passes through the basin of the solar still (state 6) to heat and raise the temperature of the saline water. This, in turns, enhances the evaporation rate of the saline water. After that, the primary flow is directed to the primary inlet port of the ejector (state g). The ejector performs the compression process by converting the enthalpy energy of the high-pressure primary flow into mechanical energy used to compress the secondary flow (explained in detail in Section 3.1).

In the present work, the generator of the ejector system is heated by hot water. The hot water is being heated by solar energy utilizing evacuated tube solar collector (ETSC). The ETSC can supply hot water with temperature higher than 373 K. To maintain continuous and stable operation, a storage tank of hot water must be included in the solar collector loop as shown in Fig. 1. On the left-hand side of Fig. 1, the solar still system consists of saline water basin with heating coil (immersed inside it), condensing chamber with cooling coil, solar still structure and glass cover to pass the solar radiation of the sun to the basin. The incident solar radiation is absorbed by the basin saline water with small part being reflected by the glass cover. With the increase of the basin temperature, the saline water starts to vaporize generating freshwater vapor (FWV). The FWV is transferred to the condensing chamber and to the inner surface of the glass cover to be condensed. The condensed water (fresh water) is collected (in a tank) for domestic use.

The proposed integrated system utilizes the solar energy to produce cold air (for air conditioning applications) and to produce fresh water. Compared to the conventional solar still, the integration of both systems makes it possible to enhance the productivity of the solar still with the addition of only two simple coils (heating and cooling coils). Furthermore, the COP of the ejector system is improved due to the further heating of the secondary flow inside the solar still. This means that there is an interactivity between the integrated solar ejector and the solar still systems as shown by Fig. 2.

3. Thermodynamics modeling

Huang (1999) presented a mathematical model for constant pressure mixing ejector. Their model predicts the ejector performance at critical-mode operation. Also, they have verified their model experimentally using 11 ejectors with R141b as working fluid. While their model was used by many published studies, the error of the model is very high and in some configurations, the resulted error reached 22%. Recently, their model was improved as discussed in detail in the review presented by Tashtoush et al. (2019b). In the present study, to simplify the integration of the ejector model with the solar still mode during the calculations of their performances, the improved ejector model developed by Huang (1999) is adapted and verified within the modeling of the solar ejector system. Also, a steady-state thermodynamic model of each system has been developed based on the conservation principles of energy, mass and momentum. This thermodynamics model of the ejector system is presented in Section 3.1 and the model of the solar still system is presented in Section 3.2.

3.1. Solar ejector system model

As shown in Fig. 3, the ejector consists of two inlet ports and one outlet port, suction chamber, constant-area section and diffuser. The high-pressure primary fluid enters the ejector at state (g), accelerates in the converging-diverging nozzle, and discharged to the suction chamber. The increase of the primary flow velocity alongside with the decrease of its pressure leads to creating a low-pressure region in the suction chamber to entrain the secondary flow at state (e). Both the primary and secondary flows are mixed (through y-m section), chocked, and discharged by the diffuser to the condenser pressure at state (c). Depending on the value of the pressure at the ejector outlet (P_c) relative to a critical value (critical backpressure P_c*) and a limited operational pressure of the condenser P_{co}, the operation of the ejector is classified into three modes:

- Critical mode (double-chocking) at $P_c < P_c$*.
- Subcritical mode (single-chocking) at P_c* $< P_c < P_{co}$.
- Back-flow mode (malfunction) at $P_{co} < P_c$.

As mentioned above, in the present system, the ejector model developed by Huang (1999) is used. This model is developed based on the following assumptions:

(1) Steady-state operation.
(2) The working fluid is an ideal gas with gas constant (R) constant specific heat (c_p), and constant specific heat ratio (γ).
(3) The kinetic energies at the inlet and exit ejector ports are negligible.
(4) The primary and secondary flows start mixing at the cross-section y-y with constant pressure $P_{py} = P_{sy}$.
(5) The entrained flow is choked at the cross-section y–y (hypothetical throat).
(6) The inner wall of the ejector is adiabatic.

Referring to Fig. 3 and the T-s diagram in Fig. 4, for a given pressure and temperature of the primary flow (P_g, T_g), the primary mass flow rate is given as:

$$\dot{m}_p = \frac{P_g A_t}{\sqrt{T_g}} \times \sqrt{\frac{\gamma}{R}\left(\frac{2}{\gamma+1}\right)^{(\gamma+1)/(\gamma-1)}} \sqrt{\eta_p} \tag{1}$$

where η_p is the isentropic efficiency of the compressible flow in the nozzle. The Mach number M_{p1}, the cross-sectional area A_{p1}, and pressure P_{p1}at the exit of the primary nozzle are related to each other using Eqs. (2) and (3):

$$\left(\frac{A_{p1}}{A_t}\right)^2 \approx \frac{1}{M_{p1}^2}\left[\frac{2}{\gamma+1}\left(1+\frac{(\gamma-1)}{2}M_{p1}^2\right)\right]^{(\gamma+1)/(\gamma-1)} \tag{2}$$

$$\frac{P_g}{P_{p1}} \approx \left(1+\frac{(\gamma-1)}{2}M_{p1}^2\right)^{\gamma/(\gamma-1)} \tag{3}$$

Through the primary flow core (section 1-1 to section y-y in Fig. 3), the Mach number M_{py} and the cross-sectional area A_{py} are calculated from Eqs. (4) and (5):

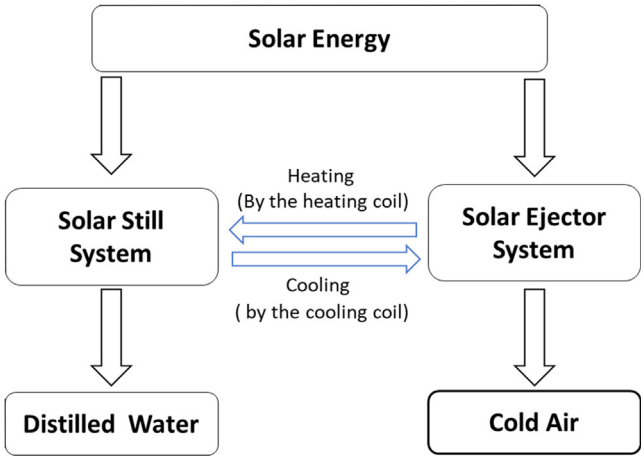

Fig. 2. The working principle of the proposed system.

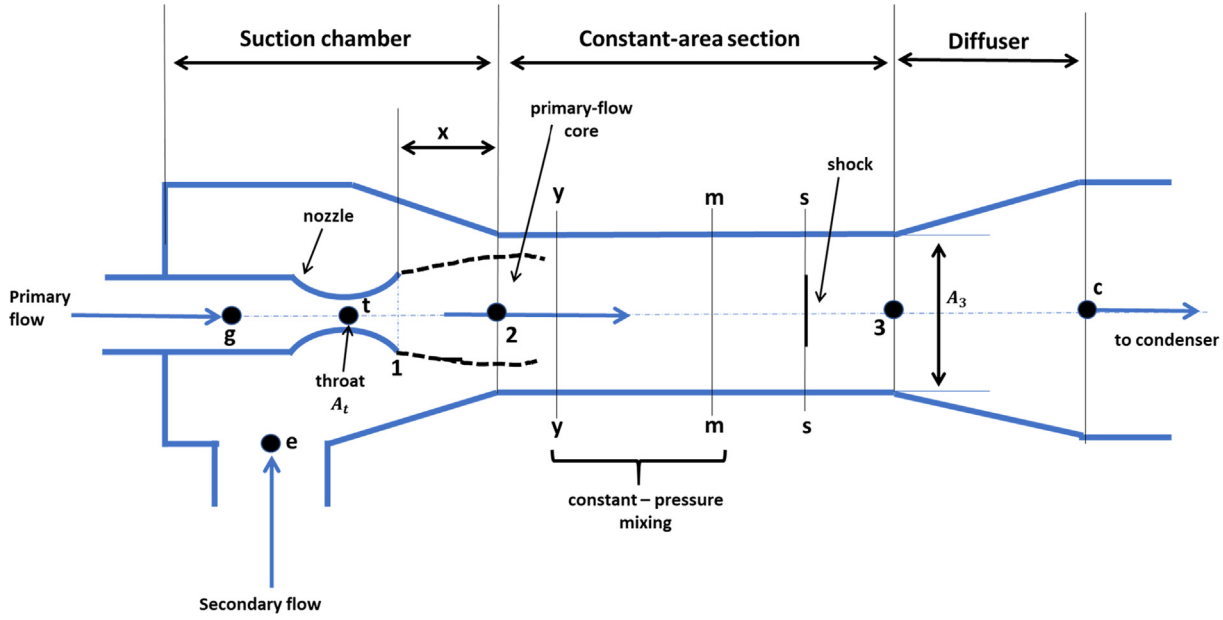

Fig. 3. Schematic diagram of the ejector.

$$\frac{P_{py}}{P_{p1}} \approx \frac{(1+\frac{(\gamma-1)}{2}M_{p1}^2)^{\gamma/(\gamma-1)}}{(1+\frac{(\gamma-1)}{2}M_{py}^2)^{\gamma/(\gamma-1)}} \tag{5}$$

$$\frac{A_{py}}{A_{p1}} \approx \frac{(\varphi_p/M_{py})[(2/(\gamma+1))\left(1+\frac{(\gamma-1)}{2}M_{py}^2\right)]^{(\gamma+1)/2(\gamma-1)}}{(1/M_{p1})[(2/(\gamma+1))\left(1+\frac{(\gamma-1)}{2}M_{p1}^2\right)]^{(\gamma+1)/2(\gamma-1)}} \tag{6}$$

where φ_p is a coefficient accounts for the losses of the main flow through the section 1-1 to y-y. The pressure of the primary flow P_{py} is equal to the pressure of the secondary flow P_{sy}. At chocking condition ($M_{sy} = 1$) and specified evaporator pressure P_e, the secondary flow pressure P_{sy} is calculated from Eq. (7):

$$\frac{P_e}{P_{sy}} \approx (1+\frac{(\gamma-1)}{2}M_{sy}^2)^{\gamma/(\gamma-1)} \tag{7}$$

Also, at the chocking condition, the secondary flow rate (entrained flow rate) is given as:

$$\dot{m}_s = \frac{P_e A_{sy}}{\sqrt{T_e}} \times \sqrt{\frac{\gamma}{R}(\frac{2}{\gamma+1})^{(\gamma+1)/(\gamma-1)}}\sqrt{\eta_s} \tag{8}$$

where η_s is the isentropic efficiency of the secondary flow.

Based on assumption 5, the cross-sectional area A_3 is calculated as the summation of the primary and entrained flow areas A_{py} and A_{sy}, respectively (as shown in Eq. (9)). However, the entrainment chocking may occur in the mixing section and the area of the entrained flow A_{sy} varies with the operational parameters as discussed by Tang et al. (2020):

$$A_3 \approx A_{py} + A_{sy} \tag{9}$$

The temperatures and Mach numbers of the primary and secondary flows at section y-y are given as:

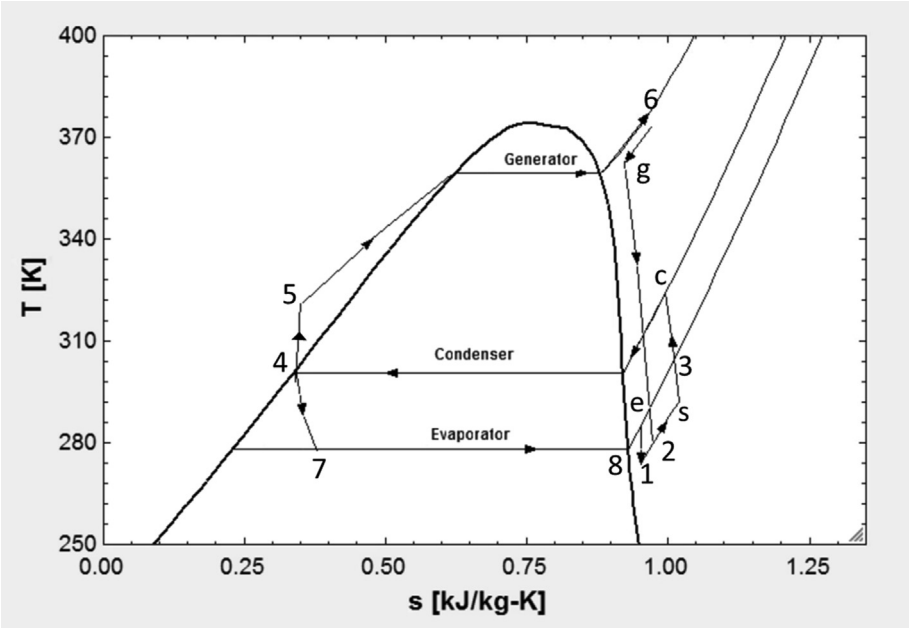

Fig. 4. T-s diagram of the ejector cooling cycle.

$$\frac{T_g}{T_{py}} = 1 + \frac{(\gamma - 1)}{2} M_{py}^2 \tag{10}$$

$$\frac{T_e}{T_{sy}} = 1 + \frac{(\gamma - 1)}{2} M_{sy}^2 \tag{11}$$

At section s-s, a chock takes place with sharp rise of the mixed flow pressure alongside with reduction in the mixed flow velocity V_m that is obtained from the conservation of momentum as expressed by Eq. (12).

$$\varphi_m [\dot{m}_p V_{py} + \dot{m}_s V_{sy}] = (\dot{m}_p + \dot{m}_s) V_m \tag{12}$$

Similarly, the temperature of the mixed flow can be obtained from the energy balance as expressed in Eq. (13):

$$\dot{m}_p \left(c_p T_{py} + \frac{V_{py}^2}{2} \right) + \dot{m}_s \left(c_p T_{sy} + \frac{V_{sy}^2}{2} \right) = (\dot{m}_p + \dot{m}_s) \left(c_p T_m + \frac{V_m^2}{2} \right) \tag{13}$$

where the gas velocities of the primary flow V_{py} and secondary flow V_{sy} at section y-y are given as:

$$V_{py} = M_{py} \times a_{py}; \quad a_{py} = \sqrt{\gamma R T_{py}} \tag{14}$$

$$V_{sy} = M_{sy} \times a_{sy}; \quad a_{sy} = \sqrt{\gamma R T_{sy}} \tag{15}$$

The Mach number of the mixed flow is given as:

$$M_m = \frac{V_m}{a_m}; \quad a_m = \sqrt{\gamma R T_m} \tag{16}$$

The pressure P_3 and Mach number M_3 at section 3-3 (inside the constant area section) are given as:

$$\frac{P_3}{P_m} = 1 + \frac{2\gamma}{\gamma + 1} (M_m^2 - 1) \tag{17}$$

$$M_3^2 = \frac{1 + (\frac{\gamma - 1}{2}) M_m^2}{\gamma M_m^2 - (\frac{\gamma - 1}{2})} \tag{18}$$

The pressure at the exit of the diffuser (state c) is calculated from Eq. (19):

$$\frac{P_c}{P_3} \approx (1 + \frac{(\gamma - 1)}{2} M_3^2)^{\gamma/(\gamma - 1)} \tag{19}$$

The performance of the ejector (as a component) is evaluated by the entrainment ratio given as:

$$\omega = \frac{\dot{m}_s}{\dot{m}_p} \tag{20}$$

While the performance of the ejector cooling cycle is expressed in terms of the coefficient of performance COP as flows:

$$COP = \frac{Q_e}{(Q_{ETC} - Q_{h,ss}) + \dot{W}_{pump}} \tag{21}$$

where Q_e is the cooling capacity of the evaporator, $\dot{W}_{pump}$ is the power consumed by the pump of the generator loop, and $Q_{h,ss}$is the heat added to the basin water of the solar still by the primary flow. Furthermore, the overall efficiency of the ejector system is given as (Varga et al., 2009):

$$\eta_{ej} = \eta_{sc} \times COP \tag{22}$$

where η_{sc} is the solar collector efficiency, which is given in terms of the optical efficiency ($F_R(\tau\alpha)$) and the loss coefficient ($F_R U_L$) as (Duffie and Beckman, 2013):

$$\eta_{sc} = F_R(\tau\alpha) - F_R U_L \left(\frac{T_{coll,in} - T_a}{G} \right) \tag{23}$$

With aid of the T-s diagram (Fig. 4) and the schematic of the integrated system (Fig. 1), the cooling capacity of the evaporator is given as (Cengel and Boles, 2015):

$$Q_e = \dot{m}_s (h_8 - h_7) \tag{24}$$

where $h_8 = h(P = P_e, x = 1)$ and $h_7 = h_4 = h(P = P_c, x = 0)$.

Defining $Q_{co,ss}$ as the heat absorbed from the condensing chamber of the solar still by the secondary flow, it can be calculated as:

$$Q_{co,ss} = \dot{m}_s cp_{8e} \Delta T_{co,ss}; \; \Delta T_{co,ss} = T_e - T_8 \tag{25}$$

where T_e is the temperature of the secondary flow at the inlet of the ejector secondary port and T_8 is the saturation temperature of the secondary fluid through the evaporator. As mentioned before, $Q_{h,ss}$ is the heat added to the basin water of the solar still by the primary flow. it is given as:

$$Q_{h,ss} = \dot{m}_p cp_{6g} \Delta T_{h,ss}; \; \Delta T_{h,ss} = T_6 - T_g \tag{26}$$

where T_6 is the temperature of the primary fluid at the outlet of the generator and T_g is the temperature of the primary flow at the inlet of the ejector primary port. Q_{ETC} is the solar heat absorbed by the evacuated tube collector (which is equal to the heat demanded by the generator). It is given as (Cengel and Boles, 2015):

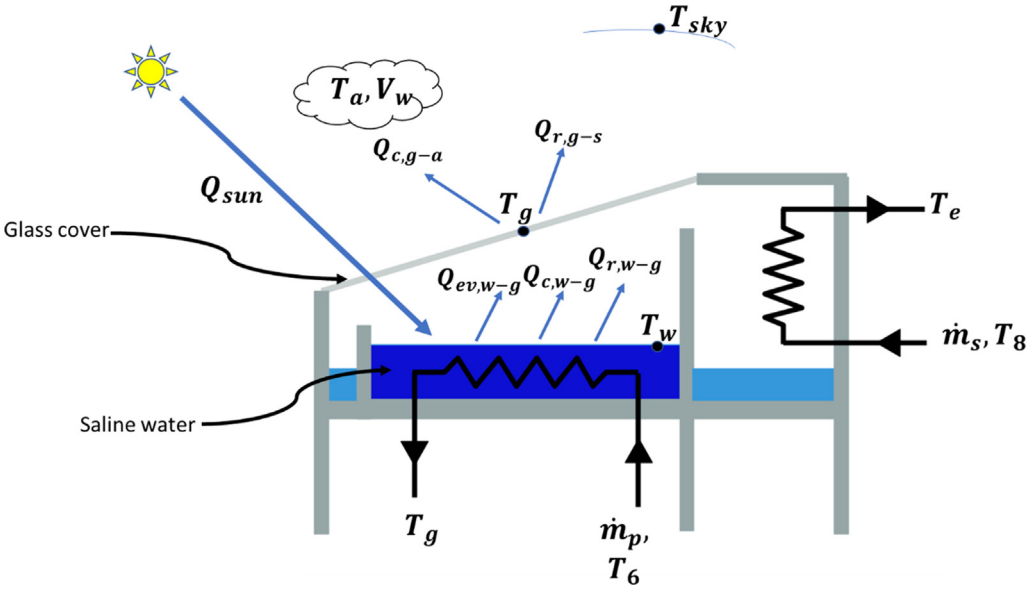

Fig. 5. Heat transfer processes of the solar still system.

$$Q_{ETC} = \dot{m}_p(h_6 - h_{5a}) \tag{27}$$

where $h_6 = h(P = P_g, T = T_6)$, h_{5a} is calculated from the isentropic efficiency of the pump:

$$\eta_{pump} = \frac{h_{5s} - h_4}{h_{5a} - h_4} \tag{28}$$

where $h_4 = h(P = P_c, x = 0)$, $h_{5s} = h(P = P_g, s = s_4)$, $s_4 = s(P = P_c, x = 0)$. Also, the Q_{ETC} can be expressed in terms of the solar collector efficiency and surface area as:

$$Q_{ETC} = \frac{G \times A_{sc}}{\eta_{sc}} \tag{29}$$

where G is the solar radiation of the sun, A_{sc} is the surface area of the solar collectors that receive the solar radiation, and η_{sc} is the efficiency of the solar collectors.

3.2. Solar still system model

In this section, the thermodynamics model of the solar still is presented. This model is developed based on the energy balance of the heat transfer processes over the saline water and the glass cover of the still, see Fig. 5. The following assumptions were made:

- Steady-state operating conditions.
- Small glass cover thickness and small depth of the saline water (less than 20 cm).
- The heat losses through the solar still walls are neglected.

The energy balance over the saline water of the solar still is expressed as (see Fig. 5):

$$Q_{sun} + Q_{h,ss} - (Q_{ev,sw-gl} + Q_{c,sw-gl} + Q_{r,sw-gl}) = 0 \tag{30}$$

where Q_{sun} is the heat absorbed by the saline water from the incident solar radiation. It is given as:

$$Q_{sun} = \tau_{gl}\alpha_w A_{sw} G \tag{31}$$

Also, the saline water absorbs more heat from the heating coil by the pass of the primary flow of the ejector system $Q_{h,ss}$ (given in Eq. (24)). $Q_{r,sw-g}$ is the radiative heat loss that transfers from the saline water to the glass cover. It is given as (Cengel and Ghajar, 2015):

$$Q_{r,sw-gl} = \varepsilon_{sw-gl}\sigma A_{sw}(T_{sw}^4 - T_{gl}^4) \tag{32}$$

$Q_{c,sw-gl}$ is the heat loss from the saline water to the glass cover that is being transferred by convection. It is given as (Cengel and Ghajar, 2015):

$$Q_{c,sw-gl} = h_{c,sw-gl}A_{sw}(T_{sw} - T_{gl}) \tag{33}$$

$Q_{ev,sw-gl}$ is the evaporative heat transfer rate from the saline water to the glass cover and condensing chamber. It is the useful form of the heat transfer from the saline water and it is given as (Cengel and Ghajar, 2015):

$$Q_{ev,sw-gl} = h_{ev,sw-gl}A_{sw}(T_{sw} - T_{gl}) \tag{34}$$

where $h_{ev,sw-gl}$ is the evaporative heat transfer coefficient from the saline water and given as (Kumar and Tiwari, 1996):

$$h_{ev,sw-gl} = 16.273 \times 10^{-3} \times h_{c,sw-gl} \times \left[\frac{P_{sw} - P_{gl}}{T_{sw} - T_{gl}}\right] \tag{35}$$

P_{sw}, P_{gl} are the effective saturated vapor pressure at the saline water temperature T_{sw} and glass cover temperature T_{gl}, respectively. They are given as (Sampathkumar et al., 2010):

$$P_{sw} = \exp\left[25.317 - \left(\frac{5144}{T_{sw}}\right)\right] \tag{36}$$

$$P_{gl} = \exp\left[25.317 - \left(\frac{5144}{T_{gl}}\right)\right] \tag{37}$$

The $h_{c,sw-gl}$ is the coefficient of the convective heat transfer from the saline water to the glass cover. It is given as in Dunkle's model (Sampathkumar et al., 2010):

$$h_{c,sw-gl} = \frac{k_v}{L_v} \times C(Gr{\cdot}Pr)^n \tag{38}$$

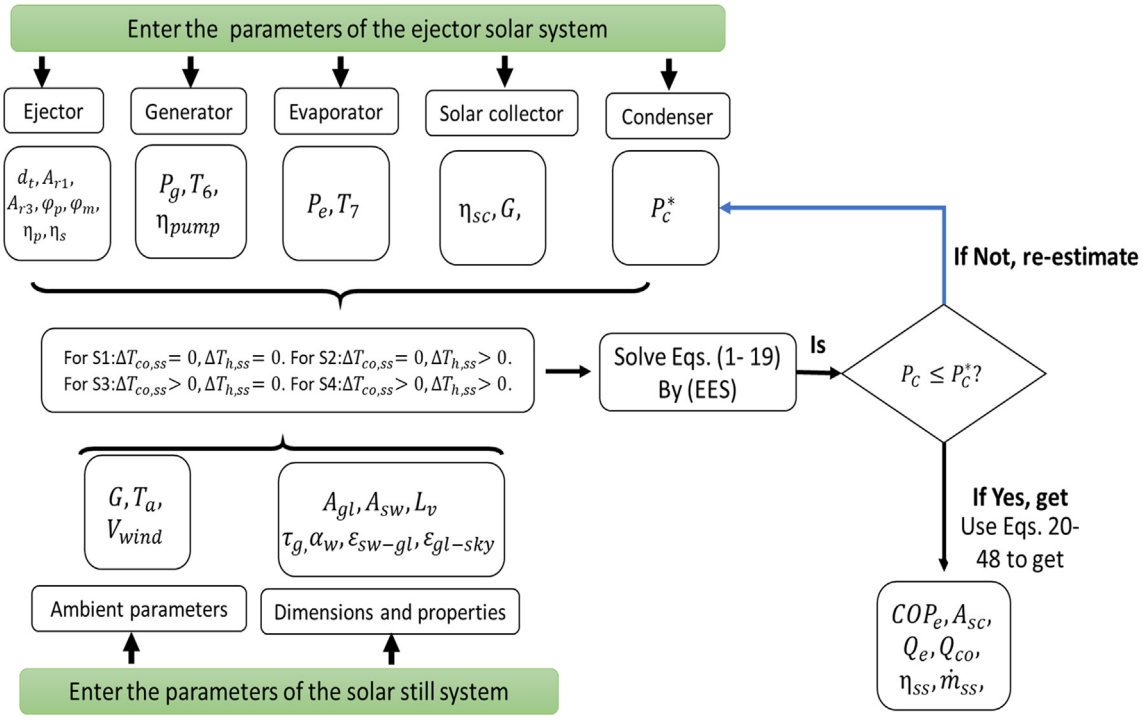

Fig. 6. Simulation procedures of the integrated system.

$$Gr = \frac{\beta g L_v^3 \rho_v^2 \Delta T}{\mu_v^2} \quad (39)$$

$$Pr = \frac{\mu_v cp_v}{k_v} \quad (40)$$

$$\Delta T = (T_{sw} - T_{gl}) + \frac{(P_{sw} - P_{gl})(T_{sw})}{(268.9 \times 10^3 - P_{sw})} \quad (41)$$

Now, the energy balance over the glass cover and the cooling coil of the solar still is expressed as:

$$Q_{ev,sw-gl} + Q_{c,sw-gl} + Q_{r,sw-gl} - (Q_{co,ss} + Q_{c,gl-a} + Q_{r,gl-sky}) = 0 \quad (42)$$

where $Q_{co,ss}$ is the heat absorbed by the secondary flow of the ejector from the condensing chamber and given in Eq. (23). $Q_{r,gl-sky}$ is the radiative heat loss from the glass cover to the sky and given as (Cengel and Ghajar, 2015):

$$Q_{r,gl-sky} = \varepsilon_{g-sky} \sigma A_{gl} (T_{gl}^4 - T_{sky}^4) \quad (43)$$

where T_{sky} is the effective sky temperature given as (Al-Nimr and Al-Ammari, 2016):

$$T_{sky} = 0.0552 \times (T_a)^{1.5} \quad (44)$$

The convective heat loss from the glass cover to the ambient air $Q_{c,gl-a}$ is given as (Cengel and Ghajar, 2015):

$$Q_{c,gl-a} = h_{c,gl-a} A_g (T_g - T_a) \quad (45)$$

where $h_{c,gl-a}$ is the coefficient of the heat transfer from the glass cover to the ambient air by convection. It is given in terms of wind speed as (Al-Nimr and Al-Ammari, 2016):

$$h_{c,gl-a} = 2.8 + 3.0 \times V_{wind} \quad (46)$$

Finally, the performance of the solar still is evaluated by the solar still efficiency and the productivity of the still per day. The solar still efficiency is given as (Al-Nimr and Al-Ammari, 2016):

$$\eta_{ss} = \frac{Q_{ev}}{G \times A_{sw} + Q_{h,ss}} \quad (47)$$

Considering that the sun is shining from i hour to j hour of the day and the enthalpy of vaporization of the water is $h_{fg,v}$, then the amount of the distilled water per day is expressed as:

$$m_{distilled} = \sum_{i}^{j} \left(\frac{Q_{ev,sw-gl,i}}{h_{fg,v,i}}\right) \times 3600 \quad (48)$$

where i to j is the hour in the day (7:00, 8:00, .., …, 17:00).

Using Eq. (48), the amount of the produced water can be calculated for each and every hour in the day, month and year for any period of interest (hourly, daily, monthly or annually).

3.3. Design point and simulation procedures

To simulate the performance of the integrated systems, the above thermodynamics models are solved using the Engineering Equation Solver (EES). Fig. 6 shows the flow chart and the steps of the simulation procedures. First, the input parameters of the ejector system and of the still system (shown in Table 1) are entered. Then, the EES automatically solves equations (1)–(19) to calculate the value of the pressure at the exit of the ejector P_c. If $P_c \leq P_c^*$, then the desired output parameters are calculated to evaluate the performance of the system. The performance of the system is studied and evaluated for four scenarios as follows:

- Scenario 1 (S1): base case scenario when ejector and solar still systems operate separately (without integration). In this scenario $\Delta T_{h,ss} = 0, \quad and \quad \Delta T_{co,ss} = 0$.
- Scenario 2 (S2): when the ejector primary flow passes through the heating coil without any flow in the cooling coil. In this scenario, $\Delta T_{h,ss} > 0, \quad and \quad \Delta T_{co,ss} = 0$.
- Scenario 3 (S3): when the ejector secondary flow passes through the cooling coil without any flow in the heating coil. In this scenario, $\Delta T_{h,ss} = 0, \quad and \quad \Delta T_{co,ss} > 0$.
- Scenario 4 (S4): when both ejector primary and secondary flows pass through heating and cooling coils, respectively. In this scenario $\Delta T_{h,ss} > 0, \quad and \quad \Delta T_{co,ss} > 0$

It is assumed that the cooling and heating coils are fabricated to meet the required temperature difference through them. To ensure the feasibility of their design, the desired temperature difference through the coils is set to be 5 K. That is, in S3 and S4, the temperature of the secondary flow at the inlet of the ejector is assumed as: $T_e = T_7 + 5K$. Where T_7 is the desired temperature of the evaporator. Similarly, the temperature of the primary flow at the inlet of the ejector in S2 and S4 is assumed as $T_g = T_6 - 5K$. Where T_6 is the temperature of the primary flow at the outlet of the generator. Also, the selected working fluid through the simulation is R134a. However, the effect of using different working fluids is discussed in Section 4.6.

4. Results and discussion

In this section, the developed model of the proposed system is validated by comparing the results of each subsystem model to published experimental results as explained in Section 4.1. Also, a parametric analysis of the major operating parameters and their effects on the performance of the system is performed by discussing the effects of the generator temperature, generator pressure, evaporator temperature, and the solar radiation of the sun. Furthermore, the effect of changing the working fluid is discussed by comparing the results of several

Table 1
Input parameters of the integrated system.

Parameter	Simulation range; (Design Value)
Solar ejector cooling system parameters	
Solar radiation intensity G (W/m^2)	500; (300–1000)
Efficiency of the evacuated tube collectors η_{sc} (%)	68
Generator pressure P_g (MPa)	3.3; (2.7–3.7)
Primary flow temperature at generator outlet T_6 (K)	365; (365–383)
Saturated temperature of the evaporator T_e (K)	283; (278–288)
Isentropic efficiency of the pump η_{pump} (%)	85
Throat diameter d_t (mm)	2.82
Area ratio (A_{p1}/A_t)	3.271
Area ratio (A_3/A_t)	9.171
Isentropic efficiency of the primary flow η_p (%)	95
Isentropic efficiency of the secondary flow η_s (%)	85
Coefficient of the frictional losses of the primary flow φ_p	0.88
Coefficient of the frictional losses of the mixed flow φ_m	0.80
Optical efficiency of the solar collectors ($F_R(\tau\alpha)$)	0.79
Loss coefficient of the solar collectors ($F_R U_L$) W/m^2-°C	5.2
Solar still system parameters	
Wind speed V_{wind} , (m/s)	5
Ambient temperature T_a, (K)	308
Transmissivity of the glass cover τ_{gl}	0.79
Surface area of the glass cover A_{gl}, (m^2)	1
Absorptivity of the saline water α_{sw}	0.90
Surface area of the saline water A_{sw}, (m^2)	1
Emissivity of the glass cover to the sky ε_{gl-sky}	1
Emissivity of the saline water to the glass cover ε_{sw-gl}	1
Average length between the glass cover and saline water L_v, (m)	0.3

working fluids at the same operating conditions.

4.1. Validation

In order to validate the results obtained by the mathematical model of the ejector system, which is solved by the EES software and its thermodynamics data, the obtained entrainment ratio are compared to experimental results obtained by Huang et al. under the same operating conditions as shown in Table 4. These results are obtained by using 11 different configurations of the ejector. Five ejectors of them have the design of nozzle A (shown in Table 2) and different constant-section diameters (shown in Table 3). The other 6 ejectors have the design of nozzle E (shown in Table 2) with different constant-section diameters (shown in Table 3). From Table 4 and Fig. 7, it can be noted that the error at higher temperature and pressure is lower than at low temperature and pressure. The resulted error ranged from 0.05 to 13.83% with an average error of 6.11%. This difference is considered acceptable taking into account the experimental uncertainty and the approximate assumptions in the ejector model. The design of ejector EF is used in the design point of this study due to its high entrainment ratio with lower error at high temperatures. The results of the solar still model in scenario 1 is compared to a set of experimental data reported by an experimental study by Madiouli et al. (2020), referred to in Table 5 as study 3. The calculated efficiency and distillation rate obtained by the present model are slightly higher than the reported experimental values in study 3 (average error of 4.56% based on the efficiency values). This may be attributed to the fact that the present model assumes no heat losses from the bottom and side walls of the still. However, as mentioned above, the results are still within the experimental uncertainty.

4.2. Effect of generator temperature

Fig. 8 shows the effect of the generator temperature on the performance of the proposed integrated solar cooling ejector system and the solar still system. The results in this section were performed under low radiant flux (500 W/m^2), representing the low average solar irradiance over the course of 1 day in desert regions such as Qatar (25°N, 51°E). The performance is expressed in terms of the coefficient of performance (Fig. 8(a)), solar still efficiency (Fig. 8(b)), solar collector area (Fig. 8(c)), and the amount of the distilled water per day (Fig. 8(d)). Notice that Eq. (48), in this particular case, takes the following form:

$$m_{distilled} = \sum_{i}^{N} \left(\frac{Q_{ev,sw-gl,i}}{h_{fg,v,i}}\right) \times 3600 = \left(\frac{500W/m^2}{h_{fg,v,i}}\right) \times 3600$$

This is because the radiant flux is taken as 500 W/m^2, representing the typical low average solar irradiance as mentioned above and it was fixed in this case to study the effect of changing the generator temperature on the performance of the system.

As shown in Fig. 7(a), the increase of the generator temperature reduces the COP of the ejector system. This explanation for this is that the increase of the generator temperature increases the entrainment ratio by the decrease of the primary flow. Comparing the COP of the various scenarios of the proposed system, S3 and S4 have the lowest COP while S1 and S2 have the highest COP. This is attributed to that the amount of secondary flow that enters the ejector in the cases of cooling the solar still (S3 and S4), is lower than the amount in cases S1 and S2, which slightly reduces the cooling capacity of the evaporator. However, the solar collector area in scenarios 2 and 4 is larger than in scenarios 1 and 2 as shown in Fig. 7(c). This is due to the heating enhancement of the still that increases the generator load and so the required solar collector area. Meanwhile, the enhancement of the condensing rate of the solar still slightly increased the load of the ejector condenser.

Fig. 8(b) shows the solar still efficiency of the various scenarios of the proposed system with solar radiation kept fixed at 500 W/m^2. It is noted that the integration of the solar still with the ejector system improves its efficiency. The efficiency of the conventional still is 38.33%. With heating enhancement (S2), the still efficiency increases to 56.37% with slight decrease with the increase of the generator temperature. With cooling enhancement (S3), the still efficiency increases to 62.8%. Both enhancements (S4) increase the efficiency to 77.95% which is about twice the efficiency of the conventional still (S1). While the efficiency of the cooling scenario (S3) is higher than of the heating scenario (S2), the productivity of the still in the heating scenario (S2) is higher than that of the cooling one (S3). This means that the effect of heating enhancement in the evaporation rate is much higher than that of the cooling enhancement effect. As shown in Fig. 8(d), the productivity of the conventional still (S1) is 1.70 kg/day. With cooling enhancement (S3), the productivity is 2.78 kg/day. The still productivity with heating scenario (S2) increases to 6.90 kg/day with decreasing trend as the generation temperature increased. The combination of heating and cooling enhancements increases the still productivity to 9.52 kg/day which is about five times higher than that of the conventional still. The decrease of the still productivity with the increase of the generator temperature in S2 and S4 is explained by the reduction of the specific heat of the working fluid at higher generator temperature. Finally, the required solar collector area increases with the increase of the generator temperature. In S2 and S4, it increases from 45.69 m^2 to 50.9 m^2 (with cooling capacity of 10.64 kW) while in S1 and S3 it increases form 43.13 m^2 to 49.35 m^2 (with cooling capacity of 10.5 kW).

4.3. Effect of generator pressure

In this section, the effect of the generator pressure on the performance of the proposed system is simulated as shown in Fig. 9. The results in this section were performed under low radiant flux (500 W/m^2), representing the low average solar irradiance over the course of 1 day in desert regions such as Qatar (25°N, 51°E). As the generator pressure increases, the driving force of the secondary flow decreases, leading to lower entrainment ratio (see Fig. 9(d)) and reduces the cooling capacity. Furthermore, the primary flow increases with the increase of the generator pressure, which leads to an increase in the generator load. Consequently, the COP of the ejector system decreases as the generator pressure increases as shown in Fig. 9(a). In contrast to ejector system, the efficiency and the productivity of the solar still are increased with the increase of the generator pressures in cases S2 and S4 that include heating enhancement as shown in Fig. 9(b, c). This is explained by that the added heat to the solar basin increases with the generator pressure as a result of the primary flow increase. Similar to the generator temperature effect, the average productivity of the solar still in S4 is 7.6 kg/day which is five times higher than that of the conventional still in S1 (1.7 kg/day). Also, the efficiency of solar still in S3 is higher than that of S2, while the productivity of the still in S2 is higher than of S3. This is because of that the cooling enhancement (S3) does not increase the load of the generator by adding more heat to the solar basin. Instead, it improves the evaporation rate by the increase of the condensation rate of the fresh water vapor. This increases the temperature difference and so the vapor pressure difference between the saline water surface and the condensation surfaces (glass cover and condensation chamber). Consequently, the driving force of the vapor transmission from the solar basin to the condensing room is increased.

Table 2
Nozzle design used in the experimental work conducted by Huang et al.

Nozzle	Throat diameter (d_t)	Exit diameter (d_{p1})	A_{p1}/A_t
A	2.64	4.50	2.905
E	2.82	5.10	3.271

Table 3
Configurations of the constant-area section of the ejectors used by Huang et al.

Name	A	B	C	D	E	F	G	H
Diameter d_3 [mm]	6.70	6.98	7.60	8.1	8.54	8.84	7.34	9.20

4.4. Effect of evaporator temperature

The evaporator temperature is one of the major parameters that affect the performance of the ejector cooling system and its cooling capacity. The results in this section were performed under low radiant flux (500 W/m^2), representing the low average solar irradiance over the course of 1 day in desert regions such as Qatar (25°N, 51°E). Following the T-s diagram shape of the wet working fluid (fluid with negative slope of the saturated-vapor line), the cooling capacity increases with the increase of the saturated evaporator temperature. Also, the saturated pressure of the evaporator increases with the increase of the evaporator temperature. This increases the secondary flow rate and further enhances the cooling capacity. Furthermore, the primary flow does not change with the increase of the evaporator temperature and the pressure at the inlet of the condenser is increased. This reduces the consumed power by the pump of the generator loop. So, the increase of the evaporator pressure increases the COP of the ejector system as shown in Fig. 10(a). It can be noted that the COP of S1 and S2 are higher than of S3 and S4. This is explained by the fact that the heating load of the generator in S3 and S4 is more than in S1 and S2.

The productivity of the still (in each scenario) was not affected by the increase of the evaporator temperature (See Fig. 10(b)). This is due to fixing the temperature differences of the secondary flow through the cooling coils to 5 K. However, the required length of the cooling coil has to be increased with the increase of the evaporator temperature to achieve the same temperature difference through the condensing chamber. This is concluded by that the increase of the evaporator temperature reduces the temperature difference between the secondary flow and the evaporated water. This leads to lower heat transfer coefficient and hence, a longer cooling coil is needed.

4.5. Effect of varying the solar radiation

The solar radiation intensity of the sun has direct effect on the required solar collector area of the ejector system and the productivity of the solar still as shown in Fig. 11(a, c). It is a straightforward result that the required solar collector area decreases with the increase of the solar radiation, see Eq. (29). The most interested point is that the required area for S2 and S4 are slightly higher than that of S1 and S3. That means the integration of the solar still with the ejector system resulted in significant enhancement of its productivity (by about five times higher than that of the conventional still) with a little penalty that is an increase in the required solar collector area. It is found that for at fixed solar collector area of 40 m^2, the cooling capacity of all scenarios (at the design point parameters) is 10.6 kW, while the still productivity was 1.72 kg/day for S1, 4.98 kg/day for S2, 2.974 kg/day for S3, and 7.08 kg/day for S4. One of the major drawbacks of the ejector systems is the dramatically reduction of their performance at the off-design conditions. To maintain a stable operation of the solar ejector system with the variation of the solar radiation, a storage tank must be incorporated to decrease the fluctuation of the primary flow temperature at the outlet of the generator. As the ambient temperature is usually high at the time of the high solar radiation, the vapor condensation process on the glass cover becomes more difficult and this minimizes the evaporation rate. However, the effect of higher solar radiation on the evaporation rate is higher than the effect of the ambient

Table 4
Comparison of the present entrainment ratio with the experimental entrainment ratio.

Ejector Name	Primary flow		Secondary flow		Experimental entrainment ratio	Present entrainment ratio	Error $= 100 \times \lvert\frac{\omega_{exp}-\omega_{th}}{\omega_{exp}}\rvert$ (%)
	T [K]	P [MPa]	T [K]	P [MPa]			
AA	368	0.604	281	0.04	0.1859	0.1804	2.96
	363	0.538	281	0.04	0.2246	0.2261	0.67
	357	0.465	281	0.04	0.288	0.292	1.39
	368	0.604	285	0.047	0.235	0.2463	4.81
	363	0.538	285	0.047	0.2946	0.3002	1.90
	357	0.4	285	0.047	0.3398	0.378	11.24
AB	363	0.538	281	0.04	0.2718	0.2701	0.63
	357	0.465	281	0.04	0.3117	0.3424	9.85
AC	368	0.604	281	0.04	0.2814	0.3128	11.16
	363	0.538	281	0.04	0.3488	0.3737	7.14
	357	0.465	281	0.04	0.4241	0.4614	8.80
AD	368	0.604	281	0.04	0.3457	0.3935	13.83
	363	0.538	281	0.04	0.4446	0.4638	4.32
	357	0.465	281	0.04	0.5387	0.5647	4.83
	368	0.604	285	0.047	0.4541	0.4949	8.98
	363	0.538	285	0.047	0.5422	0.5775	6.51
	357	0.465	285	0.047	0.635	0.6961	9.62
AG	368	0.604	281	0.04	0.2552	0.2728	6.90
	363	0.538	281	0.04	0.304	0.3292	8.29
	357	0.465	281	0.04	0.3883	0.4103	5.67
	368	0.604	285	0.047	0.3503	0.3541	1.08
	363	0.538	285	0.047	0.4034	0.4205	4.24
	357	0.465	285	0.047	0.479	0.516	7.72
EC	368	0.604	281	0.04	0.2273	0.2394	5.32
	368	0.604	285	0.047	0.304	0.315	3.62
ED	368	0.604	281	0.04	0.2902	0.3101	6.86
EE	368	0.604	281	0.04	0.3505	0.3761	7.30
EF	368	0.604	281	0.04	0.3937	0.4231	7.47
	368	0.604	285	0.047	0.4989	0.5294	6.11
EG	368	0.604	281	0.04	0.2043	0.2044	0.05
EH	368	0.604	281	0.04	0.4377	0.4817	10.05
Average error							6.11

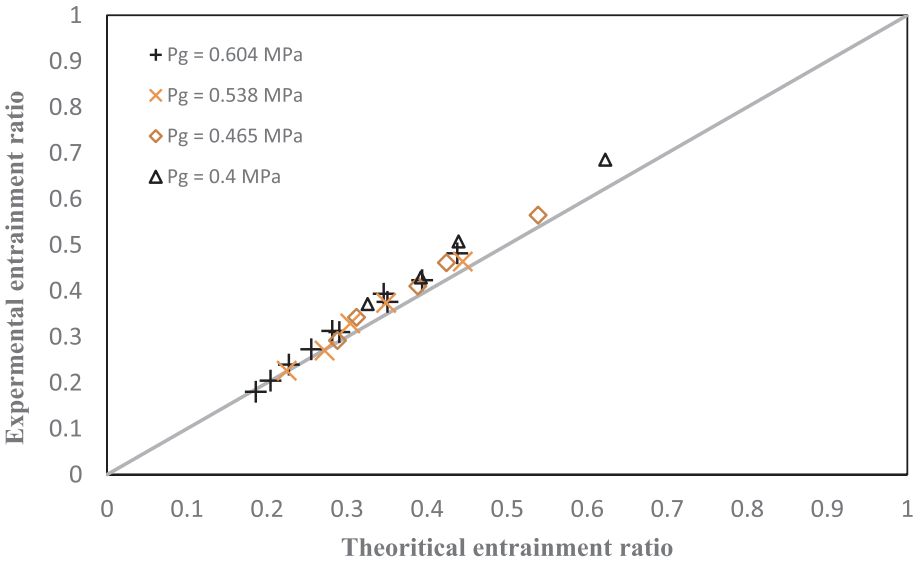

Fig. 7. Entrainment ratio comparison of present model with experimental data from Huang (1999).

Table 5
Results comparison of the present solar still model with published experimental results.

Parameter	Study 3, (Madiouli et al., 2020)	Present study
G, W/m^2	957	975
T_a, K	300	300
V_{wind}, m/s	n.a	5
A_{gl}, m^2	1	1
A_{sw}, m^2	1	1
η_{ss}, %	22	24.41
$m_{distilled}$, kg/m^2-hr	0.60	0.73

temperature on the condensation rate. This means that the still productivity increases with the increase of the solar radiation and so the solar still efficiency as shown in Fig. 11(c). Moreover, it is noted that the slop of the solar still efficiency in S1 and S3 is higher than in S2 and S4. This is explained by that the heating enhancement slightly reduces the effect of the direct solar radiation on the evaporation rate of the still and maintains the solar still efficiency nearly at constant value. In S1, as the solar radiation increases from 200 W/m^2 to 1000 W/m^2, the solar still efficiency increases from 31.8% to 46.34%. In S4, the solar still efficiency is maintained at 76% which is about 1.6 times the efficiency of S1. Also, the increase of the solar radiation improves the efficiency of the solar collectors which yields higher overall efficiency of the ejector system as shown in Fig. 11(b). Also, it can be noted that the overall efficiency of ejector system in S1 and S2 is higher than in S3 and S4 because COP of S1 and S2 is higher than that of S3 and S4.

As shown in Eq. (48), the amount of the produced distilled water varies for each hour in a day due to the variation of the solar radiation during the day and this variation is considered next. Fig. 11(d) shows the effect of the hourly variation of the solar radiation on the hourly productivity of the solar still during typical day for the time interval from 7:00 to 18:00 (10 h). The summation of the distilled water during this interval yields 3.43 kg/day for S1, 5.45 kg/day for S3, 13.20 kg/day for S2, and 18.165 kg/day for S4. This confirms that the solar still productivity in S4 is more than five times higher than in S1.

4.6. Cost estimation of the distilled water

In this section, a cost estimation of the distilled water is performed and compared to that performed by Madiouli et al. (2020). Let F to be the overall fixed cost of the solar still unit and V is the changeable cost of the still per year (assumed to be 30% of the fixed cost F). So, the overall cost of the still after N years is $C_N = F + V * N$. Also, define m_d as the distilled water produced by the still per year and the still operates for n days in the year. Here, m_d is calculated using Eq. (48) for 10 h from 7:00 AM to 5:00 PM for each operational day of the n days of the year for Qatar location. The operational days in the year, n is taken as 340 days considering 25 none operational days due to maintenance and other technical reasons. So, m_d is calculated as:

$$m_d = \sum_{1}^{n=340} (m_{distilled}) \tag{49}$$

The total distilled water by the still after N years is $m_N = m_d \times N$. Then, the estimated cost of one liter of the distilled water (for each 1 m^2 solar still area) is $C_L = C_N/m_N$. Table 5 and Fig. 12 show the estimated cost of each scenario investigated in this study compared to Conventional Solar Still (CSS) and to the system studied by Madiouli et al. (2020). The cost of a typical heating/cooling coil with total length of 15 m, outside diameter of 0.088 m, wall thickness of 3 mm and made of titanium alloy is taken as $92 (available in the market). Adding the cost of installation of the coil and required valves, it is assumed that the overall cost of each coil is $200. The solar still area is fixed at 1 m^2. It can be noted that the minimum cost of 0.033 $/kg is achieved with heating enhancement (S2) while S3 has the highest cost, see Table 5 and Fig. 12. The cost of S4 is higher than that of S2, but the produced distilled water of S4 is 1.38 times that of S2. So, the proposed system enhances the productivity of the still (by about five times in S4) and lowers the cost of the distilled water by about 30% in S2 and 15% in S4 compared to S1. The cost of one liter distilled water per 1 m^2 area of the present solar still in S4 is $0.04, while the cost of the water in the developed solar still coupled with packed bed and a parabolic trough collector presented by Madiouli et al. (2020) is $0.22 (the ratio is only 0.182), Fig. 12. This is due to the fact that the productivity of the present solar still is enhanced by improving both the evaporation rate (by heating coil) and condensation rate (by cooling coil). Furthermore, the final products of the present system are both cold air and distilled water, which reduces the cost of the heating source of the solar still by splitting it between the two systems.

It is important to state that using Eq. (49) to calculate the annual produced water (m_d) considering the hourly variation of the radiant flux during any given day in the year, resulted in water production in S4 of 5067 kg/year that is 5.7 times more than that in S1, see Table 5. While using the fixed radiant flux of 500 W/m^2 in Section 4 above to study the effect of the generator temperature, resulted in about 5 times

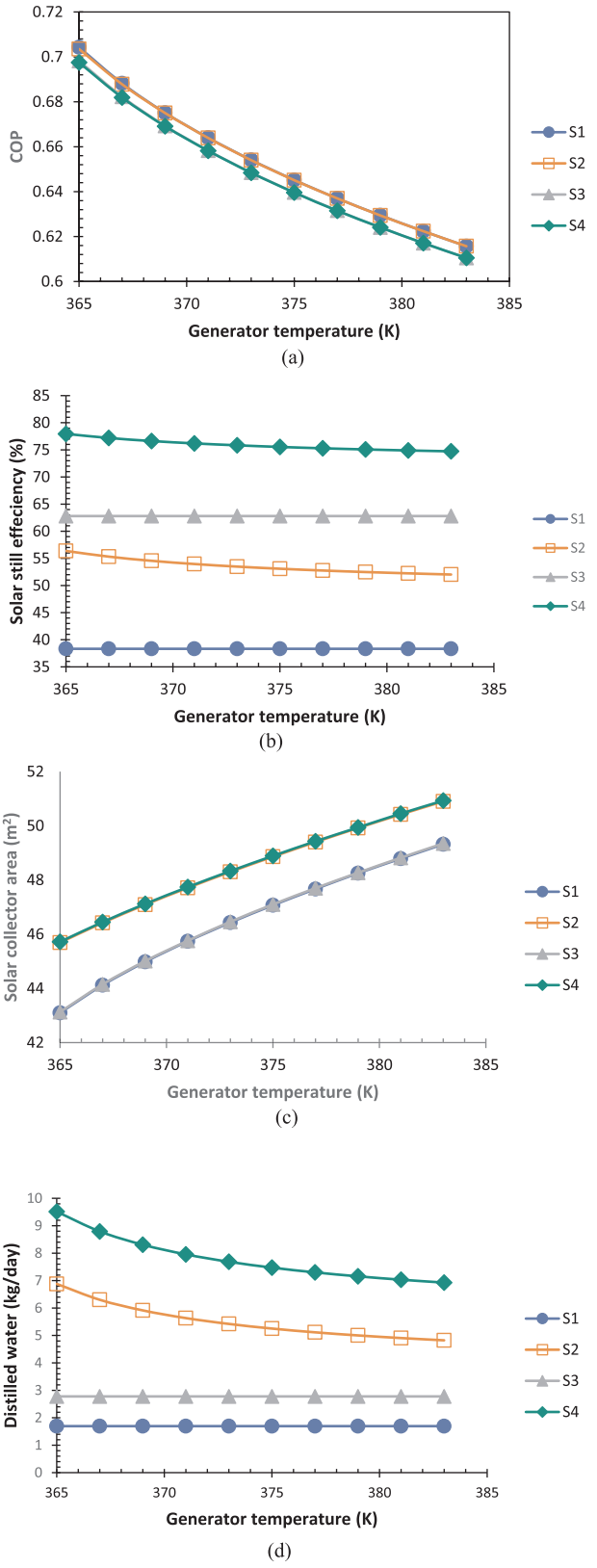

Fig. 8. Effects of the generator temperature on (a) the COP of the ejector system, (b) efficiency of the solar still, (c) solar collector area, and (d) the amount of the distilled water per day. Other input parameters are fixed at the design values (See Table 1).

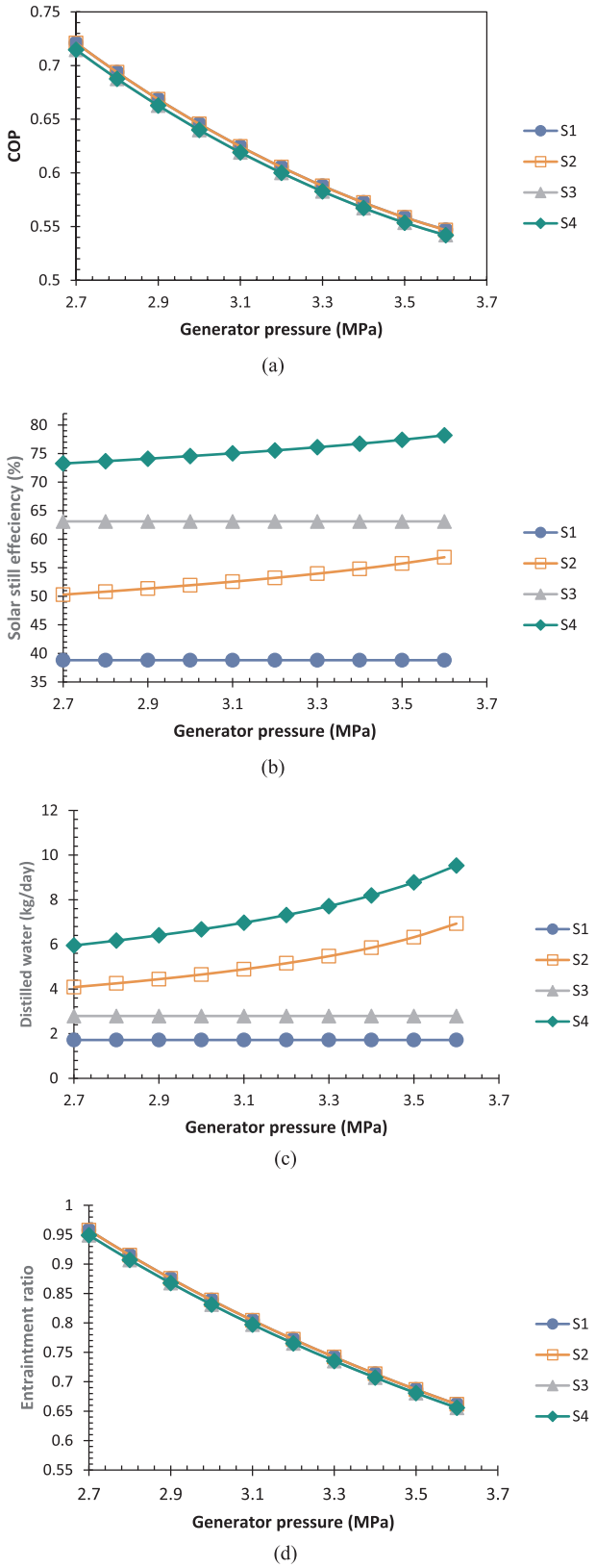

Fig. 9. Effects of the generator pressure on (a) the COP of the ejector system, (b) efficiency of the solar still, (c) the amount of the distilled water per day, and (d) the entrainment ratio. Other input parameters are fixed at the design values (See Table 1).

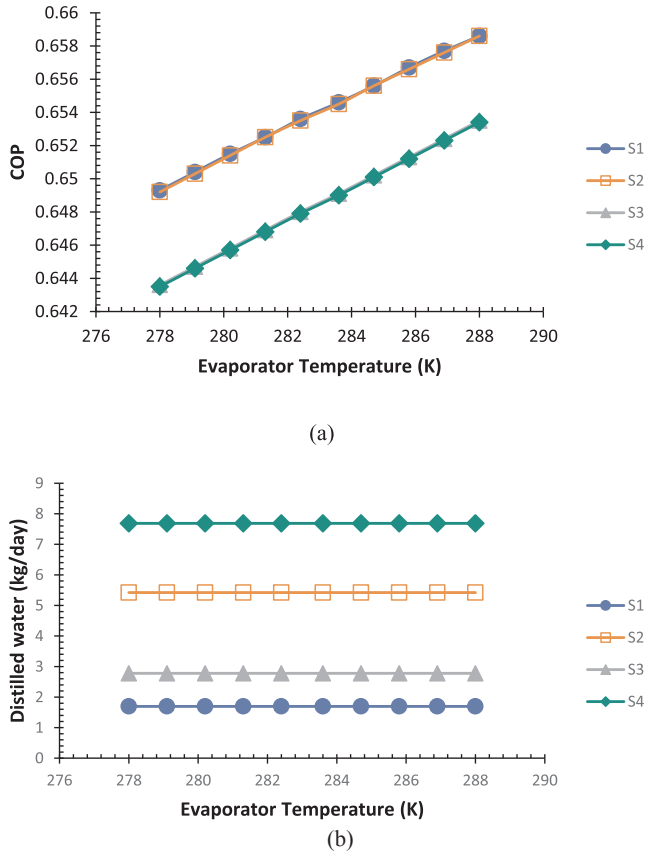

Fig. 10. Effects of the evaporator temperature on (a) the COP of the ejector system, and (b) the amount of the distilled water per day. Other input parameters are fixed at the design values (See Table 1).

improvement, indicating that the 500 W/m^2 is a conservative value.

The payback period (PBP) of the proposed scenarios compared to CSS and to the system studied by Madiouli et al. (2020) is estimated as shown in Table 6. The PBP is defined as the total cost after N year divided by the CSS cost of the yearly produced water;

PBP = $(\mathbf{C_N})/(\mathbf{C_{L,CSS}} * \mathbf{m_d})$. It should be noted that the lifetime of the CSS was taken as a reference such that its PBP equals to its lifetime. Relative to this reference, the PBP of S2 is reduced by 5 years and by 4 years for S4. This confirms that the heating enhancement (S2) is the most effective scenario in terms of cost and PBP (See Fig. 12 and Table 6).

4.7. Effect of working fluids

In this section, the effect of the working fluid on the performance of the proposed system is discussed by comparing the performance of five working fluids recommended in literature (Gupta et al., 2019; Mwesigye and Dworkin, 2018; Chen et al., 2017a; Saleh, 2016). The ejector working fluid plays a vital role in its performance. Several favourable factors should be taken into consideration through the selection of the working fluid, such as large latent heat of vaporization, large molecular mass, low viscosity, low Global Warming Potential (GWP), low Ozone Depletion Potential (ODP), stability and compatibility, non-toxic, non-explosive and the economic viability. Table 7 shows a comparison between the thermo-physical properties of the selected working fluids in this study. It should be mentioned that the working fluids of the ejector systems are usually classified into three categories (based on the slop of the saturated-vapor line in the T-s diagram): a) dry fluids (with positive slope of saturated vapor line), b) isentropic fluids (with vertical saturated vapor line), and c) wet fluids (with negative slope of the saturated vapor line).

As shown in Fig. 13(a), at the same operating conditions, R290 has the highest COP (1.26) while the R124 has the lowest COP (0.71). This is explained by the high cooling capacity of R290 relative to the required heat by the generator (See Fig. 13(b)). However, the solar collector area in case of R290 is slightly higher than required for R124 (See Fig. 13(c)). But, the high flammability of R290 makes it less favourable as a working fluid for the solar ejector. R152a has the most effect on the productivity of the solar still (as shown in Fig. 13(d)) while R142b has the least effect. In general, the performance of the wet working fluids is better than the isentropic or dry fluids. As a trade-off solution, R134a is recommended as the working fluid for its capability to achieve adequate COP with favorable environmental and safety properties (non-toxic & non-flammable) with medium GWP and zero ODP. Furthermore, it has a comparable performance to that of R290 and R152a.

5. Conclusions

A novel hybrid solar distillation and cooling system that produces both fresh water and cooling effect is proposed and investigated. The system consists of a single slope solar still coupled with solar ejector cooling system. This coupling is implemented via passing the ejector primary flow through a heating coil immersed in the basin solar still and via passing the ejector secondary flow through a cooling coil inside the condensation chamber of the still. The integration of both systems yields significant improvement in the productivity of the solar still and enhanced the COP of the ejector system. A steady state thermodynamics model of each system is developed based on the principles of momentum, energy, and mass conservations for the ejector system and based on the energy balance principle for the solar still system. The results of the model were validated against published experimental studies. Simulations were performed for four different integration scenarios; S1: the two systems operate separately, S2: the ejector primary flow passes through the heating coil only, S3: the ejector secondary flow passes through the cooling coil only and S4: ejector primary and secondary flows pass through heating and cooling coils, respectively. The effects of the major operating conditions on the performance of the system are investigated and discussed in detail. These effects include the generator pressure and temperature, evaporator temperature and solar radiation, as well as the effect of using different working fluids. Based on the results, the following is concluded:

- In scenario 4, the water productivity of the still increased by more than five times compared to the conventional still (scenario 1).
- The solar still efficiency in scenario 3 is higher than that of scenario 2. However, the still productivity in scenario 2 is higher than that of S3.
- The increase of the generator temperature, reduces the COP of the ejector system and slightly reduces the productivity of the still.
- The increase of the generator pressure, reduces the COP of the ejector and increases the productivity of the still.
- The increase of the evaporator temperature, increases the COP of the ejector system.
- For the studied working fluids (R134a, R290, R152a, R142b, R124), R290 yields the highest COP while R152a yields the highest still productivity. However, for its overall performance, safety and environmental issues, R134a is recommended.
- At a solar radiation of 500 W/m^2, generator pressure of 3.3 MPa, generator temperature of 365 K, evaporator temperature of 283 K with R134a as the working fluid, a cooling capacity of 10.54 kW, distilled water of 8.1 kg/day are obtained in S4.
- The annual produced water considering the hourly variation of the radiant flux during any given day in the year, reached 5067 kg/year in S4 that is 5.7 times more than that in S1.
- The cost of one liter distilled water per 1 m^2 area of the present solar still in S4 is $0.04, which is only a small fraction (0.18) of the cost of water produced by another technology that uses solar still coupled

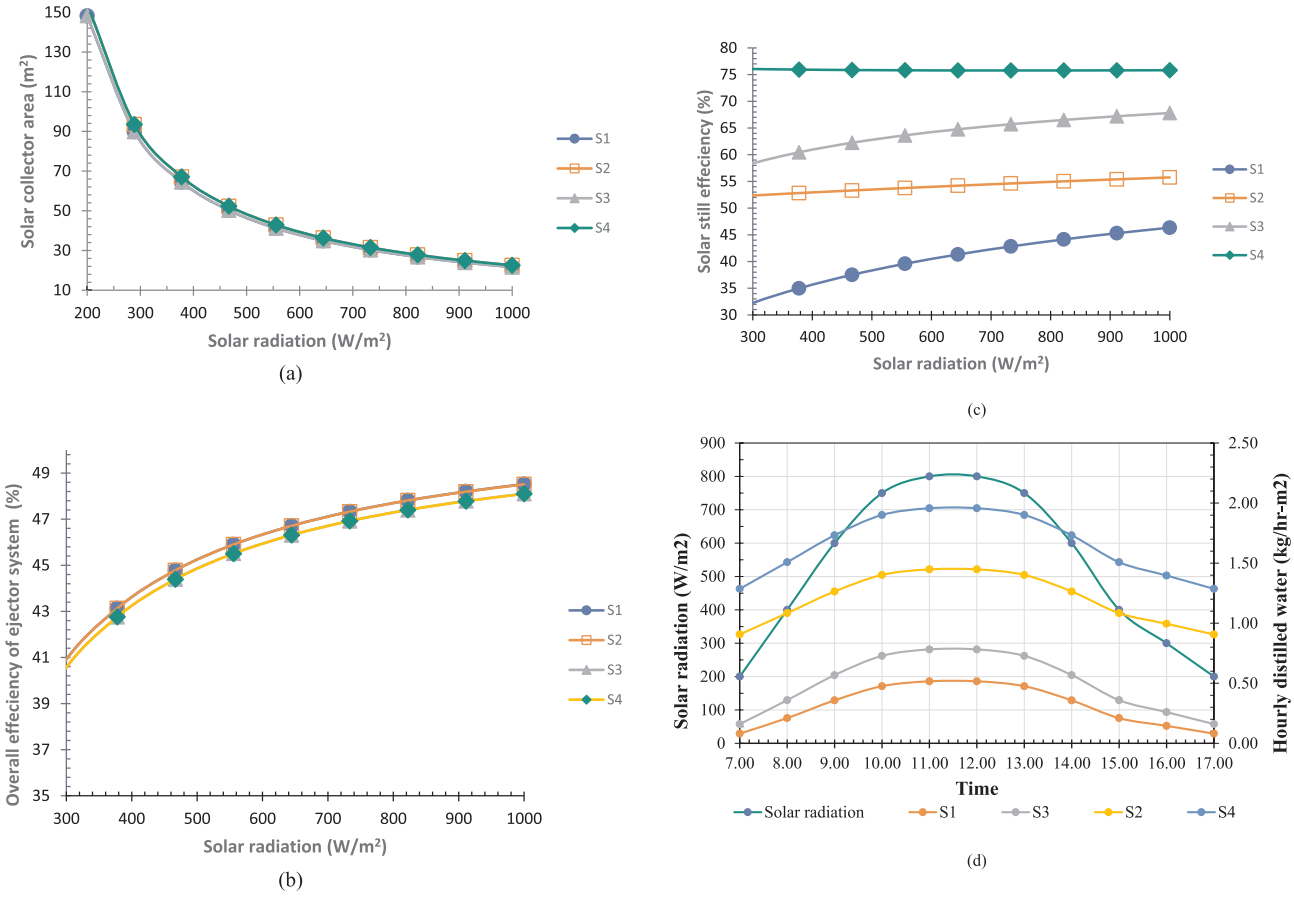

Fig. 11. Effects of the solar radiation intensity on (a) the area of the solar collector, (b) the amount of the distilled water per day, (c) overall efficiency of ejector system, and (d) hourly distilled water with the hourly variation of the solar radiation. Other input parameters are fixed at the design values (See Table 1). Data of solar hourly solar radiation is obtained from (Perez-Astudillo and Bachour, 2014).

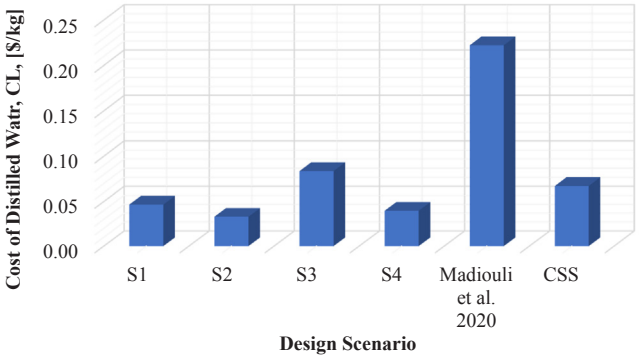

Fig. 12. Comparison of distilled water cost of 4 design scenarios of the proposed system with Madiouli et al., 2020 design and with CSS.

Table 7
Comparison between the thermo-physical properties of the selected working fluids.

Working fluid	Critical Temp. (°C)	Critical pressure (MPa)	Fluid type	GWP	ODP	Safety group
R134a	101.0	4.06	wet	1430	0	A1
R290	96.68	4.25	wet	20	0	A3
R152a	113.41	4.51	wet	124	0	A2
R142b	137.2	4.12	dry	2400	0.043	A2
R124	122.425	3.62	dry	0.06	0.026	A1

Table 6
Cost estimation of the distilled water.

Design Scenario	F ($)	V ($/year)	N (years)	m_d (kg/year)	C_N ($)	m_N (kg)	C_L ($ /kg)	Payback Period year
S1	103	30.9	10	882	412	8824	0.047	6.94
S2	303	90.9	10	3672	1212	36,723	0.033	4.90
S3	303	90.9	10	1447	1212	14,470	0.084	12.44
S4	503	150.9	10	5067	2012	50,674	0.040	5.90
Madiouli et al., 2020	850	255	10	1530	3400	15,300	0.22	33.01
CSS	103	30.9	10	612	412	6120	0.067	10

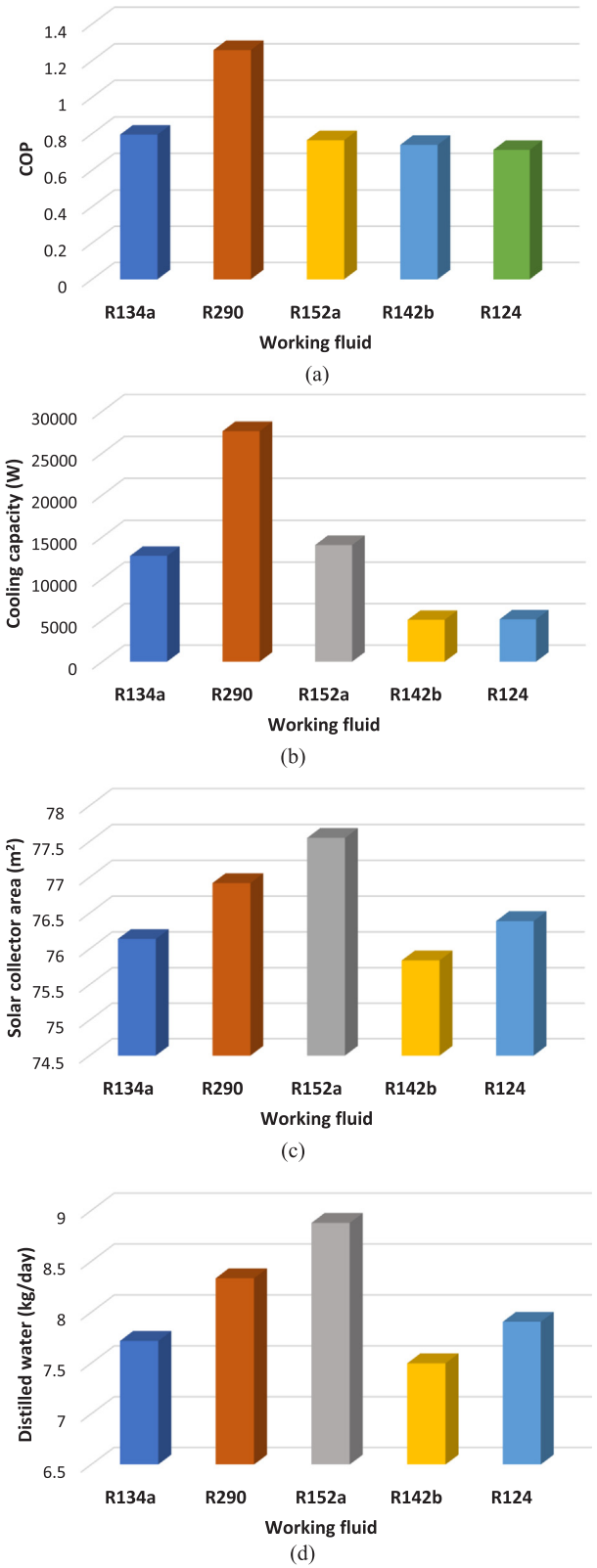

Fig. 13. Effects of the working fluids on (a) the COP of the ejector system, (b) cooling capacity, (c) solar collector area, and (d) the amount of the distilled water per day. Other input parameters are fixed at the design values (See Table 1).

with packed bed and a parabolic trough collector.

Declaration of Competing Interest

The authors declare that they have no known competing financial interests or personal relationships that could have appeared to influence the work reported in this paper.

Acknowledgement

The work presented in this publication was made possible by NPRP-S grant # [11S-1231-170155] from the Qatar National Research Fund (a member of Qatar Foundation). The findings herein reflect the work, and are solely the responsibility, of the authors.

References

Abdel-Rehim, Z.S., Lashine, A., 2012. A study of solar desalination still combined with air-conditioning system. ISRN Renew. Energy 1–7. https://doi.org/10.5402/2012/212496.

Abu-Arabi, Mousa, Al-harahsheh, Mohammad, Ahmad, Maysam, Mousa, Hasan, 2020. Theoretical modeling of a glass-cooled solar still incorporating PCM and coupled to flat plate solar collector. J. Storage Mater. 29https://doi.org/10.1016/j.est.2020.101372. (November 2019): 101372.

Al-harahsheh, Mohammad, Abu-Arabi, Mousa, Mousa, Hasan, Alzghoul, Zobaidah, 2018. Solar desalination using solar still enhanced by external solar collector and PCM. Appl. Therm. Eng. 128, 1030–1040. https://doi.org/10.1016/j.applthermaleng.2017.09.073.

Al-Nimr, Moh'd A., Al-Ammari, Wahib A., 2016. A novel hybrid PV-distillation system. Solar Energy 135, 874–883. https://doi.org/10.1016/j.solener.2016.06.061.

Al-Nimr, Moh'd Ahmad, Tashtoush, Bourhan, Hasan, Alabas, 2020. A novel hybrid solar ejector cooling system with thermoelectric generators. Energy 198. https://doi.org/10.1016/j.energy.2020.117318.

Alobaid, Mohammad, Hughes, Ben, Calautit, John Kaiser, O'Connor, Dominic, Heyes, Andrew, 2017. A review of solar driven absorption cooling with photovoltaic thermal systems. Renew. Sustain. Energy Rev. 76 (May 2016), 728–742. https://doi.org/10.1016/j.rser.2017.03.081.

Yunus, A. Cengel, Ghajar, Afshin J., 2015. Heat and Mass Transfer, Fundamentals & Application, Fifth Edition in SI Units, 5th ed. McGraw-Hill.

Cengel, Yunus A., Boles, Michael A., 2015. Thermodynamics: An Engineering Approach 8th Edition. McGraw-Hill. 10.1017/CBO9781107415324.004.

Chen, Jianyong, Havtun, Hans, Palm, Björn, 2014. Screening of working fluids for the ejector refrigeration system. Int. J. Refrig. https://doi.org/10.1016/j.ijrefrig.2014.07.016.

Chen, Jianyong, Zhu, Kangda, Huang, Yisheng, Chen, Ying, Luo, Xianglong, 2017a. Evaluation of the ejector refrigeration system with environmentally friendly working fluids from energy, conventional exergy and advanced exergy perspectives. Energy Convers. Manage. 148, 1208–1224. https://doi.org/10.1016/j.enconman.2017.06.051.

Chen, Weixiong, Shi, Chaoyin, Zhang, Shuangping, Chen, Huiqiang, Chong, Daotong, Yan, Junjie, 2017b. Theoretical analysis of ejector refrigeration system performance under overall modes. Appl. Energy. https://doi.org/10.1016/j.apenergy.2016.01.103.

Chen, Zuozhou, Xu, Jin, Shimizu, Akihiko, Hihara, Eiji, Dang, Chaobin, 2017c. Effects of the nozzle configuration on solar-powered variable geometry ejectors. Sol. Energy. https://doi.org/10.1016/j.solener.2017.04.017.

Daghigh, Roonak, Khaledian, Yavar, 2018. Effective design, theoretical and experimental assessment of a solar thermoelectric cooling-heating system. Sol. Energy 162 (October 2017), 561–572. https://doi.org/10.1016/j.solener.2018.01.012.

Das, Dudul, Bordoloi, Urbashi, Kalita, Pankaj, Boehm, Robert F., Kamble, Akash Dilip, 2020. Solar still distillate enhancement techniques and recent developments. Groundwater Sustain. Develop. 10 (July 2019), 100360. https://doi.org/10.1016/j.gsd.2020.100360.

Duffie, John A., Beckman, William A., 2013. Solar Engineering of Thermal Processes: Fourth Edition. Solar Engineering of Thermal Processes: Fourth Edition. 10.1002/9781118671603.

Ghali, K., Ghaddar, N., Alsaidi, A., 2010. Optimized operation of an integrated solar desalination and air-conditioning system: theoretical study. Renew. Energy Power Quality J. 1 (8), 169–173. https://doi.org/10.24084/repqj08.272.

Gupta, D.K., Kumar, R., Kumar, N., 2019. Development of parabolic trough collector based power and ejector refrigeration system using eco-friendly refrigerants. Progr. Solar Energy Technol. Appl. 233–308. https://doi.org/10.1002/9781119555650.ch5.

Gutiérrez, Alejandro, León, Noel, 2014. Conceptual Development and CFD Evaluation of a High Efficiency - Variable Geometry Ejector for Use in Refrigeration Applications. Energy Procedia. https://doi.org/10.1016/j.egypro.2014.10.265.

Hasanuzzaman, M., Malek, A.B.M.A., Islam, M.M., Pandey, A.K., Rahim, N.A., 2016. Global advancement of cooling technologies for PV systems: a review. Sol. Energy 137, 25–45. https://doi.org/10.1016/j.solener.2016.07.010.

Huang, B., 1999. A 1-D analysis of ejector performance analyse Unidimensionnelle de La

Performance d'un Éjecteur. Int. J. Refrig. 22 (5), 354–364. https://doi.org/10.1016/S0140-7007(99)00004-3.
Jia, Yan, Wenjian, Cai, 2012. Area ratio effects to the performance of air-cooled ejector refrigeration cycle with R134a refrigerant. Energy Convers. Manage. https://doi.org/10.1016/j.enconman.2011.09.002.
Kabeel, A.E., Harby, K., Abdelgaied, Mohamed, Eisa, Amr, 2020. A comprehensive review of tubular solar still designs, performance, and economic analysis. J. Clean. Prod. 246, 119030. https://doi.org/10.1016/j.jclepro.2019.119030.
Kumar, Sanjay, Tiwari, G.N., 1996. Estimation of convective mass transfer in solar distillation systems. Sol. Energy 57 (6), 459–464. https://doi.org/10.1016/S0038-092X(96)00122-3.
Kumar, Uday N.T., Martin, Andrew, 2014. Co-generation of drinking water and domestic hot water using solar thermal integrated membrane distillation system. Energy Procedia 61 (December), 2666–2669. https://doi.org/10.1016/j.egypro.2014.12.271.
Madiouli, Jamel, Lashin, Ashraf, Shigidi, Ihab, Badruddin, Irfan Anjum, Kessentini, Amir, 2020. Experimental study and evaluation of single slope solar still combined with flat plate collector, parabolic trough and packed bed. Sol. Energy 196 (August 2019), 358–366. https://doi.org/10.1016/j.solener.2019.12.027.
Manokar, A. Muthu, Prince Winston, D., Mondol, Jayanta Deb, Sathyamurthy, Ravishankar, Kabeel, A.E., Panchal, Hitesh, 2018. Comparative study of an inclined solar panel basin solar still in passive and active mode. Sol. Energy 169 (April), 206–216. https://doi.org/10.1016/j.solener.2018.04.060.
Mwesigye, Aggrey, Dworkin, Seth B., 2018. Performance analysis and optimization of an ejector refrigeration system using alternative working fluids under critical and subcritical operation modes. Energy Convers. Manage. 176 (August), 209–226. https://doi.org/10.1016/j.enconman.2018.09.021.
Omara, Z.M., Abdullah, A.S., Kabeel, A.E., Essa, F.A., 2017. The cooling techniques of the solar stills' glass covers – a review. Renew. Sustain. Energy Rev. 78 (October 2016), 176–193. https://doi.org/10.1016/j.rser.2017.04.085.
Opoku, R., Mensah-Darkwa, K., Samed Muntaka, A., 2018. Techno-economic analysis of a hybrid solar PV-grid powered air-conditioner for daytime office use in hot humid climates – a case study in Kumasi City, Ghana. Sol. Energy 165 (March), 65–74. https://doi.org/10.1016/j.solener.2018.03.013.
Pan, Quanwen, Peng, Jiajie, Wang, Hongbin, Sun, Haiquan, Wang, Ruzhu, 2019. Experimental investigation of an adsorption air-conditioner using silica gel-water working pair. Sol. Energy 185 (February), 64–71. https://doi.org/10.1016/j.solener.2019.04.054.
Perez-Astudillo, D., Bachour, D., 2014. DNI, GHI and DHI ground measurements in Doha, Qatar. Energy Procedia. https://doi.org/10.1016/j.egypro.2014.03.254.
Petrenko, V.O., Shestopalov, K.O., Huang, B.J., 2011. Innovative solar and waste heat driven ejector air conditioners and chillers. Ipcbee. Com 6, 338–343. http://www.ipcbee.com/vol6/no1/76-f10012.pdf.
Pounds, Daniel A., Dong, J.M., Cheng, P., Ma, H.B., 2013. Experimental investigation and theoretical analysis of an ejector refrigeration system. Int. J. Therm. Sci. https://doi.org/10.1016/j.ijthermalsci.2012.11.001.
Saengmanee, Chayarnon, Pianthong, Kulachate, Seehanam, Wirapan, Sriveerakul, Thanarath, 2017. Effects of operating conditions on the ejector characteristics and heat exchanger size of refrigeration system. Walailak J. Sci. Technol.
Saleh, B., 2016. Performance analysis and working fluid selection for ejector refrigeration cycle. Appl. Therm. Eng. 107, 114–124. https://doi.org/10.1016/j.applthermaleng.2016.06.147.
Sampathkumar, K., Arjunan, T.V., Pitchandi, P., Senthilkumar, P., 2010. Active solar distillation-A detailed review. Renew. Sustain. Energy Rev. 14 (6), 1503–1526. https://doi.org/10.1016/j.rser.2010.01.023.
Sathyamurthy, Ravishankar, El-Agouz, S.A., Nagarajan, P.K., Subramani, J., Arunkumar, T., Mageshbabu, D., Madhu, B., Bharathwaaj, R., Prakash, N., 2017. A review of integrating solar collectors to solar still. Renew. Sustain. Energy Rev. 77 (October 2015), 1069–1097. https://doi.org/10.1016/j.rser.2016.11.223.
Shublaq, M., Sleiti, A.K., 2020. Experimental analysis of water evaporation losses in cooling towers using filters. Appl. Therm. Eng. 175 (5 July) 115418.
Tang, Yongzhi, Li, Yanxia, Liu, Zhongliang, Wu, Hongqiang, Fu, Weina, 2017. A novel steam ejector with auxiliary entrainment for energy conservation and performance optimization. Energy Convers. Manage. 148, 210–221. https://doi.org/10.1016/j.enconman.2017.05.076.
Tang, Yongzhi, Liu, Zhongliang, Li, Yanxia, Shi, Can, 2018c. Combined auxiliary entrainment and structure optimization for performance improvement of steam ejector with consideration of back pressure variation. Energy Convers. Manage. 166 (March), 163–173. https://doi.org/10.1016/j.enconman.2018.04.029.
Tang, Yongzhi, Liu, Zhongliang, Li, Yanxia, Hongqiang, Wu., Zhang, Xiaopeng, Yang, Nan, 2019. Visualization experimental study of the condensing flow regime in the transonic mixing process of desalination-oriented steam ejector. Energy Convers. Manage. 197 (April), 111849. https://doi.org/10.1016/j.enconman.2019.111849.
Tang, Yongzhi, Liu, Zhongliang, Li, Yanxia, Yang, Nan, Wan, Yangda, Chua, Kian Jon, 2020. A double-choking theory as an explanation of the evolution laws of ejector performance with various operational and geometrical parameters. Energy Convers. Manage. https://doi.org/10.1016/j.enconman.2020.112499.
Tang, Yongzhi, Liu, Zhongliang, Shi, Can, Li, Yanxia, 2018a. A novel steam ejector with pressure regulation to dredge the blocked entrained flow for performance improvement in MED-TVC desalination system. Energy Convers. Manage. 172 (July), 237–247. https://doi.org/10.1016/j.enconman.2018.07.022.
Tang, Yongzhi, Liu, Zhongliang, Shi, Can, Li, Yanxia, 2018b. A novel steam ejector with pressure regulation to optimize the entrained flow passage for performance improvement in MED-TVC desalination system. Energy 158, 305–316. https://doi.org/10.1016/j.energy.2018.06.028.
Tashtoush, Bourhan M., Al-Nimr, Moh'd A., Khasawneh, Mohammad A., 2019a. A comprehensive review of ejector design, performance, and applications. Appl. Energy 240 (May 2018), 138–172. https://doi.org/10.1016/j.apenergy.2019.01.185.
Tashtoush, Bourhan M., Al-Nimr, Moh'd A., Khasawneh, Mohammad A., 2019b. A comprehensive review of ejector design, performance, and applications. Appl. Energy 240 (January), 138–172. https://doi.org/10.1016/j.apenergy.2019.01.185.
Varga, Szabolcs, Oliveira, Armando C., Diaconu, Bogdan, 2009. Analysis of a solar-assisted ejector cooling system for air conditioning. Int. J. Low-Carbon Technol. 4 (1), 2–8. https://doi.org/10.1093/ijlct/ctn001.
Wu, Hongqiang, Liu, Zhongliang, Han, Bing, Li, Yanxia, 2014. Numerical investigation of the influences of mixing chamber geometries on steam ejector performance. Desalination. https://doi.org/10.1016/j.desal.2014.09.002.
Xu, Z.Y., Wang, R.Z., 2018. Comparison of absorption refrigeration cycles for efficient air-cooled solar cooling. Sol. Energy 172 (April), 14–23. https://doi.org/10.1016/j.solener.2018.04.004.
Yan, Jia, Lin, Chen, Cai, Wenjian, Chen, Haoran, Wang, Hao, 2016. Experimental study on key geometric parameters of an R134A ejector cooling system. Int. J. Refrig. https://doi.org/10.1016/j.ijrefrig.2016.04.001.
Yan, Jiwei, Chen, Guangming, Liu, Chengyan, Tang, Liming, Chen, Qi, 2017. Experimental investigations on a R134a ejector applied in a refrigeration system. Appl. Therm. Eng. https://doi.org/10.1016/j.applthermaleng.2016.09.046.
Yapici, R., Ersoy, H.K., Aktoprakoğlu, A., Halkaci, H.S., Yiğit, O., 2008. Experimental determination of the optimum performance of ejector refrigeration system depending on ejector area ratio. Int. J. Refrig. https://doi.org/10.1016/j.ijrefrig.2008.02.010.
Zeyghami, Mehdi, Yogi Goswami, D., Stefanakos, Elias, 2015. A review of solar thermo-mechanical refrigeration and cooling methods. Renew. Sustain. Energy Rev. https://doi.org/10.1016/j.rser.2015.07.011.
Zhang, Wei, Ma, Xiaoli, Omer, S.A., Riffat, S.B., 2012. Optimum selection of solar collectors for a solar-driven ejector air conditioning system by experimental and simulation study. Energy Convers. Manage. 63, 106–111. https://doi.org/10.1016/j.enconman.2012.02.026.
Zhou, Mengliu, Wang, Xiao, Yu, Jianlin, 2013. Theoretical study on a novel dual-nozzle ejector enhanced refrigeration cycle for household refrigerator-freezers. Energy Convers. Manage. https://doi.org/10.1016/j.enconman.2013.04.028.
Zhu, Lin, Yu, Jianlin, Zhou, Mengliu, Wang, Xiao, 2014. Performance analysis of a novel dual-nozzle ejector enhanced cycle for solar assisted air-source heat pump systems. Renew. Energy. https://doi.org/10.1016/j.renene.2013.10.030.
Zhu, Yinhai, Cai, Wenjian, Wen, Changyun, Li, Yanzhong, 2009. Numerical investigation of geometry parameters for design of high performance ejectors. Appl. Therm. Eng. https://doi.org/10.1016/j.applthermaleng.2008.04.025.